Theoretical models for magneto-sensitive elastomers: A comparison between continuum and dipole approaches

Dirk Romeis,[1,*] Philipp Metsch,[2,†] Markus Kästner,[2,3] and Marina Saphiannikova[1,3]
[1]*Leibniz Institute of Polymer Research Dresden, Hohe Strasse 6, 01069 Dresden, Germany*
[2]*Institute of Solid Mechanics, Technische Universität Dresden, 01062 Dresden, Germany*
[3]*Dresden Center for Computational Materials Science (DCMS), TU Dresden, 01062 Dresden, Germany*
(Received 13 December 2016; published 3 April 2017)

In the literature, different theoretical models have been proposed to describe the properties of systems which consist of magnetizable particles that are embedded into an elastomer matrix. It is well known that such magneto-sensitive elastomers display a strong magneto-mechanical coupling when subjected to an external magnetic field. Nevertheless, the predictions of available models often vary significantly since they are based on different assumptions and approximations. Up to now the actual accuracy and the limits of applicability are widely unknown. In the present work, we compare the results of a microscale continuum and a dipolar mean field approach with regard to their predictions for the magnetostrictive response of magneto-sensitive elastomers and reveal some fundamental relations between the relevant quantities in both theories. It turns out that there is a very good agreement between both modeling strategies, especially for entirely random microstructures. In contrast, a comparison of the finite-element results with a modified approach, which—similar to the continuum model—is based on calculations with discrete particle distributions, reveals clear deviations. Our systematic analysis of the differences shows to what extent the dipolar mean field approach is superior to other dipole models.

DOI: 10.1103/PhysRevE.95.042501

I. INTRODUCTION

Magneto-sensitive elastomers (MSEs) represent a class of composite materials that consist of micron-sized magnetizable particles which are embedded into a nonmagnetizable polymer matrix. Due to mutual interactions of the particles, MSEs are able to change their effective material behavior reversibly if subjected to an external magnetic field. Moreover, they show a large magnetostrictive response: compared to pure ferromagnetic materials, their field-induced deformation is increased significantly, as described in Ref. [1]. This strong coupling between the magnetic and mechanical fields facilitates a variety of applications such as actuators and sensors [2,3], valves [4], or tunable vibration absorbers [5,6], to name just a few examples.

In the literature, a variety of different strategies for the modeling of MSEs can be found. A direct calculation of macroscopic quantities from the energy of the system is often based on the assumption that the magnetizable particles are point-like dipoles. It allows one to determine the effective elastic moduli as well as the magnetostrictive response of samples with different discrete particle distributions [7–12]. Additionally, a recent work shows that the application of a mean field approach with continuous distribution functions is promising, especially for the modeling of MSEs with chain-like microstructures [13]. To extend the applicability of such models to systems with higher particle volume fractions, a multipole expansion as presented in Refs. [14–17] for the simplified problem of only two interacting particles is a possible solution. Continuum approaches which have been developed for the modeling of MSEs can basically be divided into two groups. On the one hand, macroscale models often fit experimental data in order to describe the material behavior phenomenologically without resolving the microstructure [18–23]. On the other hand, microscale models as described in Refs. [24–30] allows one to determine the local magnetic and mechanical fields since particles and matrix are considered separately. Hence, no limiting assumptions regarding the magnetization have to be made. In these microscale continuum models, denoted "full field approach" in the following, macroscopic quantities are calculated by applying an appropriate homogenization scheme.

Since the individual modeling strategies differ significantly in fundamental assumptions, a comparison between different approaches is a complex task which has to be accomplished in order to identify their advantages and disadvantages as well as the limits of applicability. The aim of this work is a comprehensive comparison between the dipole interaction and the full field technique. To this end, the approaches described in Refs. [13,27] are applied and the average magnetostrictive response of MSEs with different particle volume fractions is calculated. Furthermore, comparisons with a modified dipole model, which is based on an evaluation of discrete particle distributions, are carried out to illustrate the differences compared to the mean field approach. The results are eventually used to identify to what extent the considered modeling strategies are an adequate tool to handle specific problems.

The work is structured as follows: short reviews of the applied modeling strategies are given in Secs. II and III. In Sec. IV, the mean field approach is adapted to two-dimensional problems in order to allow for a detailed comparison with the simulation results of the full field approach in Sec. V. Moreover, finite element simulations for selected particle distributions are opposed to the predictions of the discrete dipolar-interaction model in this section. After a short discussion of the results in Sec. VI, the paper is closed by concluding remarks and an outlook to necessary future work.

*romeis@ipfdd.de
†philipp.metsch@tu-dresden.de

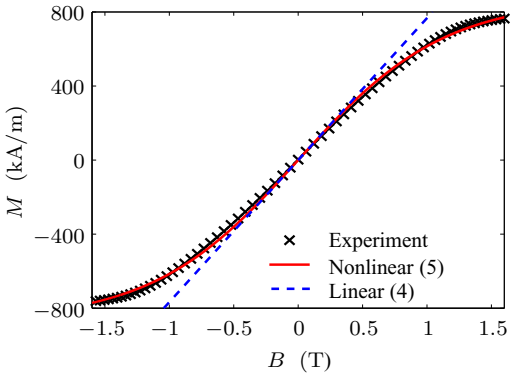

FIG. 1. Magnetization behavior of BASF CIP CC: comparison of experimental data from Ref. [33] with the models according to Eqs. (4) and (5).

II. THE FULL FIELD APPROACH

To resolve the local magnetic and mechanical fields, a continuum formulation of the coupled magnetomechanical boundary value problem is applied. Herein, the magnetizable particles and the nonmagnetizable polymer matrix are considered separately, which allows us to capture the influence of different microstructures. Macroscopic quantities such as the effective magnetostrictive strain are calculated by performing a numerical homogenization procedure as described in Refs. [27,31]. In the following, the applied full field approach is summarized: field equations that are relevant for the simulations presented in Sec. V are introduced, whereas additional relations including boundary and jump conditions are omitted for brevity. For a detailed discussion of the theoretical framework the reader is referred to Ref. [27].

In the stationary case, the magnetic part of the problem is described by the following equations [32]:

$$\nabla \cdot \boldsymbol{B} = 0, \tag{1}$$

$$\nabla \times \boldsymbol{H} = \boldsymbol{j}. \tag{2}$$

Here, the quantities $\boldsymbol{B}$, $\boldsymbol{H}$, and $\boldsymbol{j}$ denote the magnetic induction, the magnetic field, and the vector of free current density, respectively. If the relation $\boldsymbol{B} = \nabla \times \boldsymbol{A}$ is applied to derive $\boldsymbol{B}$ from the magnetic vector potential $\boldsymbol{A}$ that satisfies the Coulomb gauge condition, Eq. (1) is fulfilled automatically and only Ampère's law given by Eq. (2) remains to be solved. Another field quantity which describes the magnetic state of the material is the magnetization $\boldsymbol{M}$. It links the magnetic induction and the magnetic field via the equation

$$\boldsymbol{B} = \mu_0(\boldsymbol{H} + \boldsymbol{M}), \tag{3}$$

in which $\mu_0 = 4\pi \times 10^{-7}\ \mathrm{N\,A^{-2}}$ is the permeability of free space. While $\boldsymbol{M} = 0$ holds within the nonmagnetizable polymer matrix, the experimental data depicted in Fig. 1 show that the magnetization behavior of the carbonyl iron particles (CIPs) can be characterized by the nonlinear relation

$$M = M_\infty \tanh(\delta B), \tag{4}$$

which connects the magnitude of the magnetization and the magnetic induction. In Eq. (4), $M_\infty = 868\ \mathrm{kA\,m^{-1}}$ and $\delta = 0.883\ \mathrm{T^{-1}}$ are the saturation magnetization and a scaling parameter. Moreover, a linearization for small values of B allows us to find the expression

$$M = M_\infty \delta B = \frac{\mu_\mathrm{r} - 1}{\mu_0 \mu_\mathrm{r}} B, \tag{5}$$

in which $\mu_\mathrm{r} = 27.61$ is the relative magnetic permeability. It relates to the magnetic susceptibility via $\chi = \mu_\mathrm{r} - 1$. For illustration purposes, the models according to Eqs. (4) and (5) are also included in Fig. 1.

According to Refs. [34,35], the existence of magnetic fields entails an additional body force density $\boldsymbol{f}^\mathrm{m}$ which has to be considered in the mechanical part of the problem:

$$\boldsymbol{f}^\mathrm{m} = \boldsymbol{j} \times \boldsymbol{B} + (\nabla \boldsymbol{B})^\mathrm{T} \cdot \boldsymbol{M}. \tag{6}$$

If $\boldsymbol{f}^\mathrm{m}$ is expressed as the divergence of a magnetic stress tensor $\boldsymbol{\sigma}^\mathrm{m} = \boldsymbol{\sigma}^\mathrm{max} + (\boldsymbol{B} \cdot \boldsymbol{M})\mathbf{1} + \boldsymbol{B} \otimes \boldsymbol{M}$ in which the quantities $\boldsymbol{\sigma}^\mathrm{max}$ and $\mathbf{1}$ denote the Maxwell stress and identity tensors, the symmetric total stress tensor $\boldsymbol{\sigma}^\mathrm{tot} = \boldsymbol{\sigma}^\mathrm{m} + \boldsymbol{\sigma}$ can be introduced as the sum of the magnetic and mechanical stresses. Hence, the balance of linear momentum is given by the relation

$$\nabla \cdot \boldsymbol{\sigma}^\mathrm{tot} + \rho \boldsymbol{f} = 0 \tag{7}$$

for the stationary magnetomechanical boundary value problem. Herein, ρ and $\boldsymbol{f}$ are the mass density and the mechanical body force density, respectively. The mechanical behavior of both constituents is assumed to be elastic: a finite deformation framework for the modeling of MSEs within the full field approach is presented in Refs. [25,33]. However, in Ref. [27] it is shown that the regions where the strain is increased are comparably small if materials with a moderate particle volume fraction are considered. To this end, a linear elastic behavior leading to the relation

$$\boldsymbol{\sigma}^\mathrm{tot} = \frac{E}{1+\nu}\boldsymbol{\varepsilon} + \frac{E\nu}{(1+\nu)(1-2\nu)}\,\mathrm{tr}(\boldsymbol{\varepsilon})\mathbf{1} + \boldsymbol{\sigma}^\mathrm{max} \tag{8}$$

is applied. In Eq. (8), $\boldsymbol{\varepsilon}$ is the strain tensor, whereas the material parameters E and ν represent Young's modulus and Poisson's ratio of the individual constituents. Regarding the simulation results, $E_\mathrm{p} = 210$ GPa and $\nu_\mathrm{p} = 0.3$ have been chosen to specify the comparably stiff iron particles and $E_\mathrm{m} = 200$ kPa as well as $\nu_\mathrm{m} = 0.49$ are used to characterize the quasi-incompressible polymer matrix.

To compare the results of the full field formulation and the dipolar mean field approach that is presented in the following section, effective field quantities $\langle(\cdot)\rangle$ are calculated according to the relation

$$\langle(\cdot)\rangle = \frac{1}{V_\mathrm{s}} \int_{V_\mathrm{s}} d^3r\,(\cdot). \tag{9}$$

This can be accomplished by applying the homogenization framework illustrated in Refs. [27,31]. Thus, periodic boundary conditions are used to ensure the equivalence of microscopic and macroscopic energies as described in Ref. [36]. While, for accuracy, it is advantageous to resolve the local magnetic and mechanical fields, a major drawback of the full field approach is the high computation time that is needed to generate the results. In the present work, this issue is overcome by limiting the simulations to two dimensions. Consequently, the magnetizable particles have to be considered

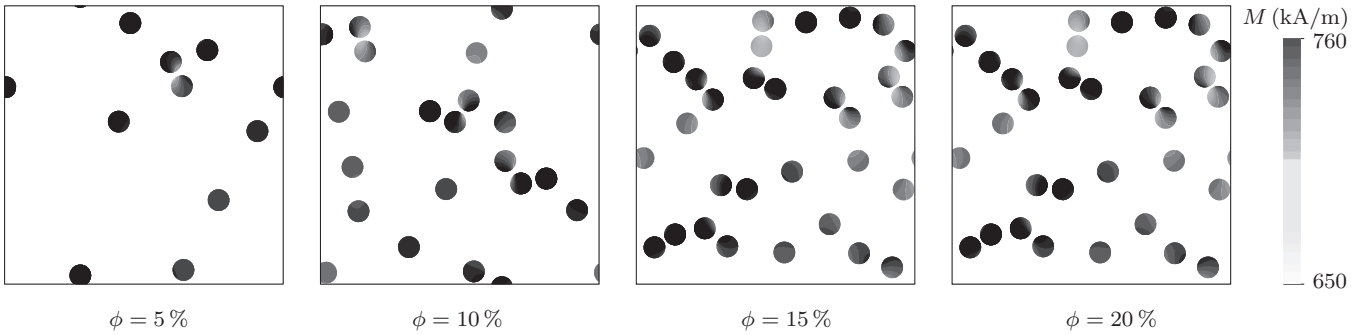

FIG. 2. Distribution of the magnetization for randomly generated microstructures with a varying particle volume fraction ϕ in a magnetic field of 1 T oriented in horizontal direction to the sample: the simulation results show that the probability to find a homogeneously magnetized particle is higher in dilute systems—for larger values of ϕ, nearly all particles exhibit an inhomogeneous magnetization.

as infinitely long cylinders while any out-of-plane deformation is prevented—a similar modeling strategy is described in Ref. [37]. To allow for magnetostrictive strains in the finite element calculations, a rectangular macroscopic body that is magnetized homogeneously in the external magnetic field is assumed. Additionally, the effective Maxwell stress outside the material is prescribed as a macroscopic load. This approach neglects perturbations of the macroscopic fields within the sample and is similar to those used in Refs. [27,38,39].

Figure 2 depicts simulation results which have been obtained for randomly generated particle distributions with a volume fraction ϕ varying from 5 % to 20 %. Each picture shows the distribution of the magnetization within a representative volume element if a macroscopic magnetic induction $\langle B \rangle = 1$ T is applied in the horizontal direction. The periodic boundary conditions result in mutual interactions of the magnetizable particles beyond the boundaries. It is visible that there are many particles which can be considered as homogeneously magnetized for dilute systems with $\phi = 5\,\%$ and $\phi = 10\,\%$. Here, the average distance between the particles is comparably high. In contrast, their compact arrangement in the representative volume elements with $\phi = 15\,\%$ and $\phi = 20\,\%$ entails an inhomogeneous magnetization. Accordingly, an assumption of magnetic dipoles might not be considered valid anymore.

For the comparisons in Sec. V, 20 different realizations of such representative volume elements are evaluated in order to determine the average behavior of MSEs with random isotropic particle distributions of a specific volume fraction. Additionally, the finite element results for the discrete particle distributions depicted in Fig. 2 are compared with the predictions of the modified dipole model. This allows us to highlight the differences of the mean field and discrete approaches.

III. DIPOLAR MEAN FIELD APPROACH

In a previous work [13] we described our mean field method in detail, so we only sketch it here briefly. Essentially we introduce some additional simplifying approximations in comparison to the full field approach.

First, the magnetic interactions among the incorporated microparticles are described via mutually interacting magnetic dipoles. This reduces the computational effort considerably because we do not resolve the magnetization field inside the inclusions explicitly. Formally, for each particle $i \in [1,\mathcal{N}_\mathrm{p}]$ we sum up the original magnetization field $\boldsymbol{M}(\boldsymbol{r})$ into a single dipole moment $\boldsymbol{m}_i$ located in the particle center $\boldsymbol{r}_i$:

$$\boldsymbol{m}_i = \int_{v_i} d^3r\, \boldsymbol{M}(\boldsymbol{r}), \tag{10}$$

where v_i denotes particle volume. Thus, the dipole $\boldsymbol{m}_i$ represents the average magnetization of a particle, $\boldsymbol{M}_i = \boldsymbol{m}_i/v_i$. Approximation of the "true" electromagnetic field in the sample by mutually interacting dipoles is well established in the literature [7–12,40,41]. Commonly, each particle is assigned the same dipole moment, which is obtained self-consistently in the field generated by all the other identical dipole moments, $\boldsymbol{m}_i = \boldsymbol{m}$ ($\forall\ i$). In previous works [11,13] it has been emphasized that this assumption is only strictly valid in the case of a homogeneous external field applied to an ellipsoidal sample, where the particles are locally arranged in such a way that all of them have an identical neighborhood. For example, this is the case if the particles are ordered on a regular lattice [7–12,40,41] or if an amorphous microstructure, i.e., a random isotropic distribution, is assumed [13,41]. Assigning all particles the same dipole moment was termed as the mean field assumption in Ref. [41]. In contrast, in our previous work [13] we characterize the spatial distribution of particles or dipoles via a continuous dimensionless distribution function $\Phi_\mathrm{p}(\boldsymbol{r})$ and explicitly calculate a position-dependent magnetization $\boldsymbol{M}(\boldsymbol{r})$ as a self-consistent functional of $\Phi_\mathrm{p}(\boldsymbol{r})$; see Eqs. (11) and (12). This "smearing" or "averaging" of the possible neighboring positions in terms of a "mean" concentration field $\Phi_\mathrm{p}(\boldsymbol{r})$ we denote as the dipolar mean field approach.

In the present work we only consider the case of a random isotropic microstructure, with homogeneous $\Phi_\mathrm{p}(\boldsymbol{r}) = \phi_0$. Consequently, also the magnetization field is homogeneous, i.e., position independent, and each particle would have the same dipole moment $\boldsymbol{m}_i = \boldsymbol{m}$ in Eq. (10). Together with the affine deformation assumption (except at very short ranges) the present approach employed for magnetostriction seems to be very similar to the one presented in Ref. [41] for electrostriction of an amorphous microstructure. However, some conceptual differences remain. First of all, the authors in Ref. [41] consider exclusively linear polarization, whereas we extend our model to saturating magnetization behavior. Second, Ref. [41] focuses on the field-induced changes in the local material properties but does not account explicitly for

the effects of the macroscopic sample deformation onto the local properties. Furthermore, it is assumed that the dipoles displace affinely on all length scales, which is accounted for in the two-particle distribution function.

In contrast to Ref. [41], we consider in detail the interplay between microstructure effects and macroscopic effects [13]. Moreover, it is known that, at very short ranges, the two-particle distribution function is affected by hard-sphere packing effects. We propose that, in this case also, nonaffine deformation processes become important. We do not make any further considerations about these processes but assume them to preserve the form of the microstructure locally [13]. This allows us to simplify the calculations considerably. Thus, with respect to the local redistribution effects the model in Ref. [41] differs essentially from the present one.

For a given $\Phi_p(\boldsymbol{r})$ the magnetization is obtained self-consistently via the relations

$$\boldsymbol{M}(\boldsymbol{r}) = \boldsymbol{X}(\boldsymbol{H}(\boldsymbol{r})) = \boldsymbol{X}(\boldsymbol{H}_0(\boldsymbol{r}) + \boldsymbol{H}_d(\boldsymbol{r})), \tag{11}$$

$$\boldsymbol{H}_d(\boldsymbol{r}) = -N_d\boldsymbol{M}(\boldsymbol{r}) + \int_{V_s} \frac{d^3r'}{4\pi}\Theta\left(\Delta r^2 - d_p^2\right) \times \Phi_p(\boldsymbol{r'})\frac{3[\boldsymbol{M}(\boldsymbol{r'})\cdot\Delta\boldsymbol{r}]\Delta\boldsymbol{r} - \Delta r^2\boldsymbol{M}(\boldsymbol{r'})}{\Delta r^5}. \tag{12}$$

Here, $\Delta\boldsymbol{r} = \boldsymbol{r} - \boldsymbol{r'}$ and $\boldsymbol{X}(\boldsymbol{H})$ is a material function describing the particles magnetization behavior. For isotropic linear magnetization $\boldsymbol{X}(\boldsymbol{H}) = \chi\boldsymbol{H}$, see Eq. (5) with $B = \mu_0\mu_r H$. The parameter N_d denotes the single-particle (self-)demagnetization factor, which is $N_d = 1/3$ for spheres. Thus, the (otherwise diverging) contribution from the interaction of a particle or dipole with itself is excluded from the integral on the right-hand side in Eq. (12) via the Heaviside step function Θ. The particle diameter d_p takes the role of a short-range cutoff to prevent particle overlap.

The magnetic interaction energy within the MSE sample exerted to a homogeneous external magnetic field $\boldsymbol{H}_0$ is then calculated as [13]

$$U_{mag} = \mu_0\int_{V_s} d^3r\left\{\frac{1}{2}\boldsymbol{M}(\boldsymbol{H} - \boldsymbol{H}_0) - \int_0^H \boldsymbol{M}d\boldsymbol{H}\right\}. \tag{13}$$

Furthermore, we describe the elastic energy in the sample via the Neo–Hooke law for an incompressible body [42]:

$$U_{el} = \frac{E_s}{6}\left((1+\varepsilon)^2 + \frac{2}{1+\varepsilon} - 3\right). \tag{14}$$

Here, $\varepsilon = \Delta L_\parallel/L_{\parallel_0}$ denotes the relative change of the length of the sample in the direction of the applied field $\boldsymbol{H}_0$. With $L_\perp$ denoting the size of the sample perpendicular to $\boldsymbol{H}_0$, the aspect ratio of an incompressible sample before ($\Gamma_0 = L_{\parallel_0}/L_{\perp_0}$) and after ($\Gamma = L_\parallel/L_\perp$) the deformation is related to ε via

$$\Gamma = \Gamma_0(1+\varepsilon)^{3/2}. \tag{15}$$

The elastic modulus E_s in Eq. (14) represents an effective parameter describing the elastic properties of the sample as a whole, the polymeric network plus incorporated rigid particles. For low volume fraction ϕ of spherical particles, the effective modulus of the filled network can be approximated via [43]

$$E_s = E_m(1 + 2.5\phi), \tag{16}$$

where E_m denotes the elastic modulus of the pure polymer phase.

The third fundamental approximation we introduce is the assumption that all particles can only "move" affinely relative to the deformation of the sample as a whole. This affine approximation is, just like the dipole approximation [15–17], very reasonable for long distances between particles. If the particles come very close to each other our assumptions must fail. As explained in our previous work [13], we summarize the present approximation as the neglect of short-range effects. Particularly, if the amount of magnetizable particles in the sample is low $\phi \ll 1$, we expect our approach to describe the behavior of MSEs correctly.

Depending on a "start" configuration of the sample (particle distribution Φ_p and sample aspect ratio $\Gamma = L_\parallel/L_\perp$) we calculate the deformation $\langle\varepsilon\rangle$ which minimizes the total energy of the sample at given $\boldsymbol{H}_0$:

$$u_{tot} = u_{mag} + u_{el}. \tag{17}$$

Here, $u = U/V_s$ is the corresponding energy per sample volume.

IV. ADAPTATION OF DIPOLE APPROACH

As already mentioned in Sec. II, the finite element simulations performed in the full field model assume the field variables to be constant in the third dimension. This corresponds to a sample containing infinitely long cylinders aligned parallel to each other and the external magnetic field directing orthogonal to the cylinders main axis. In contrast, the dipolar mean field approach was developed for microspheres dispensed in a sample that is varying or deforming in the third dimension as well. In the following we present a corresponding adaptation of our dipolar mean field approach to the systems considered in Sec. II.

A. Magnetic contribution

We assume the cylinders to be aligned in the z direction. Analogously, we assume constant magnetization in that direction [$\boldsymbol{M} \neq \boldsymbol{M}(z)$] and the components of all fields are restricted to the plane perpendicular to z. Furthermore, the distribution function Φ_p is also constant in z (perfect parallel alignment) and the cutoff d_p now refers to the cross-sectional diameter of a cylinder. To account for the magnetization at some position z' and its influence on a reference position in the plane $z = 0$ we perform the integration with respect to $z' \to \pm\infty$ in Eq. (12) and directly obtain

$$\boldsymbol{H}_d(\boldsymbol{s}) = -N_d\boldsymbol{M}(\boldsymbol{s}) + \int_{A_s} \frac{d^2s'}{2\pi}\Theta\left(\Delta s^2 - d_p^2\right) \times \Phi_p(\boldsymbol{s'})\frac{2[\boldsymbol{M}(\boldsymbol{s'})\cdot\Delta\boldsymbol{s}]\Delta\boldsymbol{s} - \Delta s^2\boldsymbol{M}(\boldsymbol{s'})}{\Delta s^4}. \tag{18}$$

Here, $\boldsymbol{s} = x\boldsymbol{e_x} + y\boldsymbol{e_y} = \boldsymbol{r}$ ($z = 0$) spans the two-dimensional (2D) plane perpendicular to the cylinders main axis. A magnetizable infinitely long cylinder with its main axis perpendicular to the magnetic field has a demagnetization factor $N_d = 1/2$ [44]. This particular derivation of the interaction

of magnetic dipoles in a plane is owed to our mean field description using a dimensionless continuous distribution function for the positions of the dipoles. In Appendix A we demonstrate that this is analogous to the case of a chain of n_z dipoles with a line density n_z/L_z in the third (z) direction and it is also identical to a homogeneously magnetized circle in a 2D plane.

In the following we assume that all fields (i.e., $\boldsymbol{M}$, $\boldsymbol{H}$, $\boldsymbol{B}$) are aligned parallel to the homogeneous external field $\boldsymbol{H}_0$. In the dipole approach we use H_0 to control the strength of the magnetic interaction in the sample. In contrast, in our full field approach in Sec. II the control parameter is defined as the effective induction $\langle B\rangle$ in the sample; see Eq. (9). Accordingly, $\langle B\rangle$ can be calculated from the contributions in the magnetizable particles $\langle B_\mathrm{p}\rangle$ and in the nonmagnetizable matrix $\langle B_\mathrm{m}\rangle$:

$$\langle B\rangle = \phi\langle B_\mathrm{p}\rangle + (1-\phi)\langle B_\mathrm{m}\rangle. \tag{19}$$

With $\langle B_\mathrm{p}\rangle = \mu_0(\langle H\rangle + \langle M\rangle)$ and $\langle B_\mathrm{m}\rangle = \mu_0(H_0 + \phi\langle M\rangle f_\mathrm{macro})$ we obtain

$$\langle B\rangle = \mu_0 H_0 + \mu_0\phi\langle M\rangle(1 - N_\mathrm{d} + f_\mathrm{macro}). \tag{20}$$

We discuss f_macro explicitly in Sec. IV C; for details see Ref. [13]. For linear magnetization ($M = \chi H$) this reduces to

$$\langle B\rangle = \mu_0 H_0 \frac{1 + \chi_\mathrm{eff}\phi(1-N_\mathrm{d})}{1 - \chi_\mathrm{eff}\phi f_\mathrm{macro}}, \tag{21}$$

with $\chi_\mathrm{eff} = \chi/(1 + N_\mathrm{d}\chi)$. So we obtained a relation between $\langle B\rangle$ and H_0. It is worth considering these relations in more detail. With $H_0 = H - H_\mathrm{d}$ and $M = \chi H$, Eq. (20) may be equally written as

$$\langle B\rangle = \mu_0\langle M\rangle\left(\frac{1}{\chi} + N_\mathrm{d} + \phi(1-N_\mathrm{d})\right). \tag{22}$$

This is a remarkable result because it directly relates the average magnetization of the particles to the effective induction in the sample. Within our dipole approach the magnetization is the central quantity which is calculated self-consistently for a given external field H_0. The magnetization crucially depends on the sample shape as well as on the local particle distribution Φ_p [11,13]. From Eq. (22) we note that $\langle B\rangle$ immediately fixes the average magnetization $\langle M\rangle$ and vice versa, independent of the sample details. We could likewise interpret $\langle B\rangle$ as a self-consistent parameter as well. But one must be aware that, although the derivation from Eq. (19) to Eq. (22) is obtained strictly by fundamental magnetostatics, it is a direct consequence of our dipole approximation assuming the magnetic fields within any individual particle to be homogeneous. We emphasize that our dipole approach [13] still accounts for different average magnetizations in each particle. Hence, deviations from the analytic relation (22) must be due to inhomogeneities of the magnetization field in the particles and it provides a first simple measure for the accuracy of the dipole approach. Furthermore, in the full field approach $\langle B\rangle$ is fixed "externally" and it is assumed to be the same in the entire sample. With Eq. (22) this corresponds to a constant average magnetization in the entire sample. This will prove to be very helpful when considering rectangular samples.

B. Elastic contribution

The sample is assumed to remain fixed in the z direction ($\Delta L_z = 0$). This corresponds to the plain-strain condition in the theory of continuum mechanics [45]. Again we assume an incompressible and isotropic sample. Then the aspect ratio before, Γ_0, and after, Γ, deformation is related via

$$\Gamma = \Gamma_0(1+\varepsilon)^2, \tag{23}$$

and the Neo–Hooke law from Eq. (14) changes to

$$U_\mathrm{el} = \frac{E_\mathrm{s}}{6}\left((1+\varepsilon)^2 + \frac{1}{(1+\varepsilon)^2} - 2\right). \tag{24}$$

Note that the prefactor $1/6$ in Eqs. (14) and (24) is identical, since for plain-strain conditions the shear modulus remains constant $G^{(3\mathrm{D})} = G^{(2\mathrm{D})}$ [45]. The effective elastic modulus E_s for a medium containing infinitely long rigid cylinders is given in the dilute limit ($\phi \ll 1$) by [45]

$$E_\mathrm{s} = E_\mathrm{m}(1 + 2\phi). \tag{25}$$

The parameter E_m again denotes the elastic modulus of the pure matrix phase.

C. Results for random isotropic distribution

Similar to Ref. [13] we describe a random isotropic distribution via a constant distribution function $\Phi_\mathrm{p}(\boldsymbol{r}) = \phi$. In the thermodynamic limit of a macroscopic sample ($L_\parallel, L_\perp, \mathcal{N}_\mathrm{p} \to \infty$ at given ϕ) we can safely neglect finite size effects arising at the sample boundaries. As a first example we consider the MSE sample to form an ellipse in the xy plane. Analogous to an ellipsoidal sample in 3D [11,13,44,46], an elliptic sample of homogeneously magnetized material also generates a homogeneous demagnetization field $\boldsymbol{H}_\mathrm{d} \parallel \boldsymbol{M}$ [and with Eq. (11) also $\boldsymbol{M} \parallel \boldsymbol{H}_0$] in its interior. For a random isotropic distribution (no internal microstructure [13]), the magnetization of each particle is then the same in every point of the sample, and accordingly $M(\boldsymbol{s}) = \mathrm{const.} = \langle M\rangle$. Like in Ref. [13] we define the shape effect f_macro by the integral expressions in Eq. (18):

$$H_\mathrm{d} = -N_\mathrm{d}M + \phi\langle M\rangle f_\mathrm{macro}. \tag{26}$$

With the (arbitrary) reference point in the center ($\boldsymbol{s} = 0$) of the elliptic sample we have

$$f_\mathrm{macro}^\mathrm{ellipse} = \int_1^\Gamma \frac{4ds'}{2\pi s'}\int_0^{\theta(s')} d\theta'(2\cos^2\theta' - 1), \tag{27}$$

with

$$\theta(s') = \sin^{-1}\left(\frac{1}{s'}\sqrt{\frac{\Gamma^2 - s'^2}{\Gamma^2 - 1}}\right),$$

and Γ the aspect ratio of the ellipse. This can be solved analytically:

$$f_\mathrm{macro}^\mathrm{ellipse} = \frac{1}{2}\frac{(\Gamma-1)^2}{\Gamma^2 - 1}. \tag{28}$$

For a linear magnetization behavior ($M = \chi H$) we obtain the self-consistent magnetization from Eq. (11):

$$\langle M\rangle = \frac{\chi H_0}{1 + \chi N_\mathrm{d} - \chi\phi f_\mathrm{macro}}. \tag{29}$$

This represents a general result for linear magnetization [13]. With $M = \langle M\rangle$ being the same in every magnetizable particle and zero otherwise, the volume integral in Eq. (13) just provides an additional factor ϕV_s. For linear magnetization behavior, Eq. (13) reduces to [13]

$$u_\mathrm{mag} = \frac{U_\mathrm{mag}}{V_\mathrm{s}} = -\frac{\mu_0}{2}\phi H_0\langle M\rangle. \tag{30}$$

Since $f_\mathrm{macro}^\mathrm{ellipse}$ in Eq. (28) is monotonically increasing with the aspect ratio Γ, the MSE sample will always tend to elongate in direction of the applied field $\boldsymbol{H}_0$. The same qualitative behavior is also obtained for 3D samples with magnetizable rigid spheres being randomly isotropic distributed [13].

In the full field approach in Sec. II a rectangular unit cell with periodic boundary conditions in the x and y direction is considered; see Fig. 2. Thus, the sample itself should be regarded of a rectangular form as well. For rectangles in 2D, as for cuboids in 3D, the implied homogeneity of the demagnetization field inside the sample can no longer be strictly valid. However, to compare both approaches we note that, in the full field approach, we assumed a constant effective (or average) magnetic induction $\langle B\rangle$ in each unit cell and hence in the entire sample. For a representative segment, or unit cell, of such an MSE sample this is reasonable, if the segment itself is considered to be located "deep" inside the sample. With Eq. (22) we equally assume a constant average magnetization $\langle M\rangle$ throughout the sample. For a random isotropic distribution $[\Phi_\mathrm{p}(\boldsymbol{s}) = \phi]$ we again have $M = \mathrm{const.} = \langle M\rangle$ in the direction of the external field. Within our dipolar mean field approach we consider a single-particle "deep" in the sample, i.e., the center itself, as a representative unit and apply the boundaries of a rectangle in Eq. (18):

$$f_\mathrm{macro}^\mathrm{rectangle} = \frac{1}{2\pi}\int_{-L_\perp/2}^{L_\perp/2} dy' \int_{-L_\parallel/2}^{L_\parallel/2} dx' \frac{x'^2 - y'^2}{(x'^2 + y'^2)^2}\Theta\left(s'^2 - d_\mathrm{p}^2\right). \tag{31}$$

Noting that the integral vanishes over a perfect square ($L_\perp = L_\parallel$ or $\Gamma = 1$) as well as it does over a perfect circle, the integrals in Eq. (31) can be greatly simplified. The result reads

$$f_\mathrm{macro}^\mathrm{rectangle} = \frac{2}{\pi}[\tan^{-1}(\Gamma) - \tan^{-1}(1)]. \tag{32}$$

In Fig. 3 we show the results for both shape effects f_macro of a rectangular and an elliptic sample as well as our previous result for a 3D spheroid. In the upper part of Fig. 3 we plot f_macro directly as a function of Γ, displaying the actual similarity among all of them. In any case we always predict an elongation in direction of the applied field $\boldsymbol{H}_0$ as they all monotonically increase with respect to Γ. Furthermore, all curves intersect in the point $\Gamma = 1$ (perfect symmetric sample), where f_macro vanishes. In the lower part of Fig. 3 we plot the derivative with respect to ε at $\varepsilon = 0$ (and thus fixed initial aspect ratio Γ_0). The quantity $\partial f_\mathrm{macro}/\partial\varepsilon|_{\varepsilon=0}$ represents a direct measure for the internal force deforming the sample at a given external field [13]. Here, clear differences between

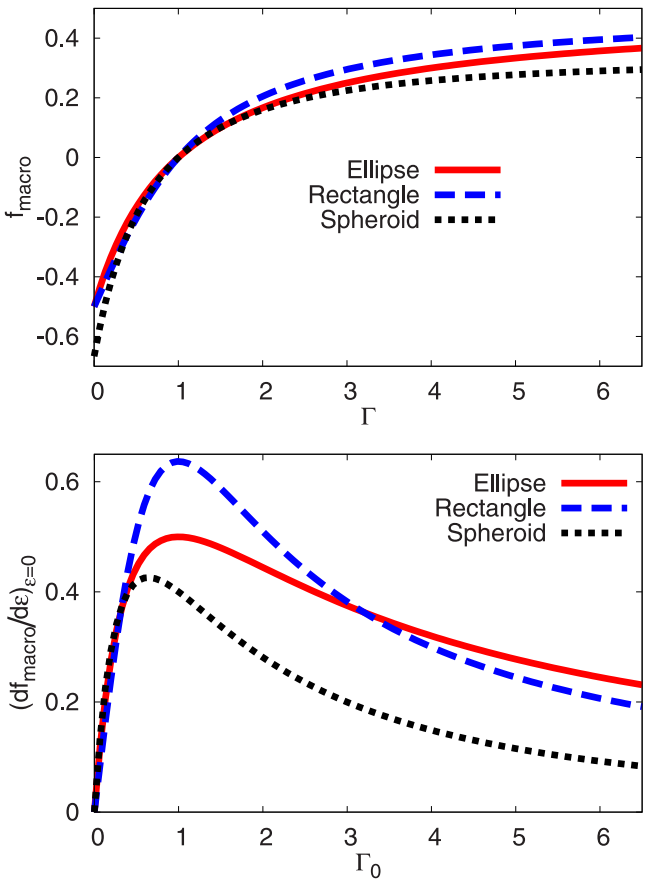

FIG. 3. In the upper plot the functions f_macro for an elliptic and a rectangular sample are shown. For comparison we also display our result for a 3D spheroidal sample [13]. In the lower plot the corresponding changes at infinitesimal deformation are illustrated.

the samples become obvious. Note that the deformation force in elliptic and rectangular samples are maximal exactly at $\Gamma_0 = 1$, whereas in spheroidal samples the maximal force is found around $\Gamma_0 \approx 0.7$.

D. Saturating magnetization behavior

We insert Eq. (3) into Eq. (4) to model saturating magnetization behavior in terms of the magnetic field H. To obtain the magnetic energy Eq. (13) we make use of the bijective property of Eq. (4) to calculate the total differential dH/dM and change integration variable in Eq. (13) $dH \to dM$. The result reads

$$u_\mathrm{mag} = \frac{U_\mathrm{mag}}{V_\mathrm{s}} = \frac{\mu_0\phi}{2}\left\{(1 - N_\mathrm{d} + \phi f_\mathrm{macro})\langle M\rangle - \frac{1+\chi}{\chi}\ln\left(1 - \frac{\langle M\rangle^2}{M_\infty^2}\right)\right\}. \tag{33}$$

From Eqs. (18) and (4) the self-consistent magnetization M and its average value $\langle M\rangle$ are obtained, respectively. Finally, to relate the external magnetic field H_0 to the effective induction $\langle B\rangle$ we can use the general equation (20) again. Adapting Eq. (22) to the present saturating magnetization behavior, the

relation $\langle B\rangle(\langle M\rangle)$ reads

$$\langle B\rangle = \mu_0 M_\infty \left\{ \frac{1+\chi}{\chi} \tanh^{-1}\left(\frac{\langle M\rangle}{M_\infty}\right) - (1-N_d)(1-\phi)\frac{\langle M\rangle}{M_\infty} \right\}. \quad (34)$$

Again, this is independent of the sample shape or the particle distribution Φ_p.

V. COMPARISON OF RESULTS

We now compare the deformation behavior and the magnetization behavior in direction of the applied magnetic field as predicted by both approaches. The comparison for the average behavior is carried out for linear as well as for saturating magnetization behavior, whereas the results for some selected discrete particle distributions are only presented for linear magnetization.

A. Random isotropic distributions

In Fig. 4 the average outcomes from the full field approach (for 20 different randomly generated systems) are compared to the analytic dipolar mean field calculations. The dashed lines represent the dipolar mean field prediction and the squares, with corresponding statistical error bars, display the results obtained in our full field approach. Here, no fitting or adjusting of any variable in the corresponding theories has been applied. Both approaches assume identical system parameters (i.e., see the caption in Fig. 4). With this in mind and recognizing the fundamental different concepts and approximation schemes applied in both approaches, the notable agreement of the results is astonishing. In the upper plot of Fig. 4 we show the effective deformation $\langle\varepsilon\rangle$ in direction of the applied magnetic field for different volume fractions ϕ of magnetizable particles in the sample. Except for the results with $\phi = 15\%$ both approaches coincide almost perfectly to each other. But even here the dipolar mean field result is found within the standard deviation from the full field calculations. In the lower plot of Fig. 4 we compare the effective magnetization within the sample $\langle M_s\rangle = \phi\langle M\rangle$ in dependence of the applied effective induction $\langle B\rangle$ for both approaches. The dipolar mean field approach predicts the relation Eq. (22) independent of the explicit shape of the sample or of the distribution function Φ_p. From our full field calculations we obtain quite perfectly the identical relation for each ϕ. It is also worth to note that, in contrast to the upper plot in Fig. 4, the error bars for the average magnetization are vanishingly small. This supports the mean field picture Eq. (22) of an identical magnetization (at given $\langle B\rangle$) in the sample independent of the explicit particle distribution.

In Fig. 5 we present the same results for a saturating magnetization scheme according to Eq. (4). In the full field approach the same 20 systems are considered as in the case of linear magnetization. Hence it is not surprising that the degree of conformity between the results of our two approaches is almost identical to the case of linear magnetization. Nevertheless, in Fig. 5 we prove that the quantitative correspondence also holds for a realistic magnetization behavior. Note, that the present choice for μ_r and M_∞ very accurately describes the magnetization behavior that has been observed in experiments

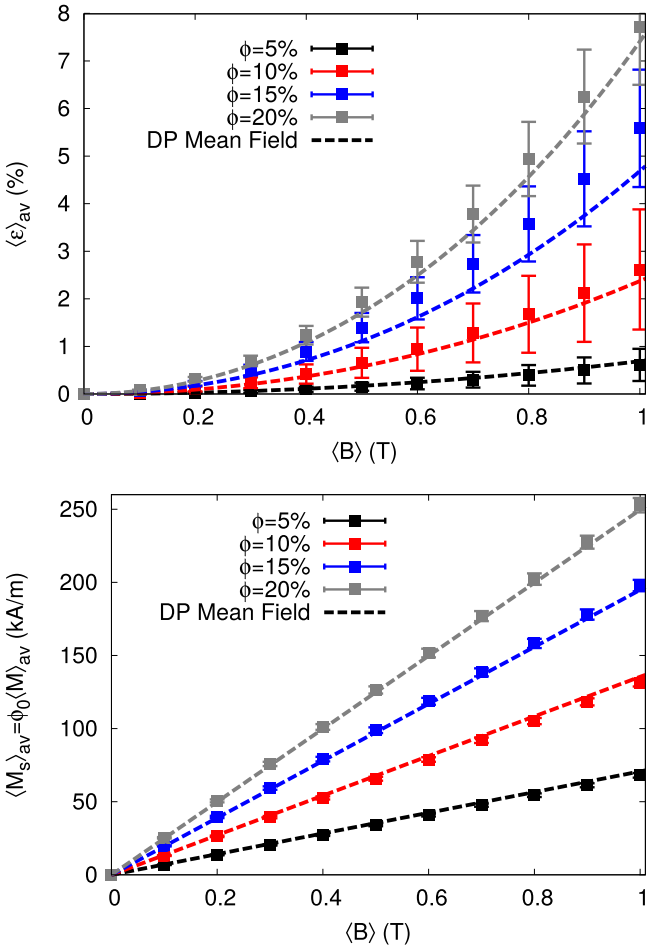

FIG. 4. Comparison of the results for different volume fraction ϕ of linearly magnetizable particles in the sample. In the upper plot the effective deformation $\langle\varepsilon\rangle_{av}$ (averaged over 20 samples) in direction of the applied field H_0 ($\langle B\rangle$) is shown. In the lower plot the corresponding averaged effective magnetization $\langle M_s\rangle_{av}$ in the samples is shown. Parameters are $\mu_r = \chi + 1 = 27.61$ and $E_m = 200$ kPa.

for carbonyl iron powder [33] (Fig. 1). For $\langle B\rangle \leqslant 0.3$ Tesla the results in Fig. 5 resemble those in Fig. 4. At increasing applied magnetic fields especially the magnitude of deformation is notably reduced for the saturating magnetization behavior.

B. Discrete particle positions

In Appendix B we shortly explain how we obtain the results for explicit particle distributions within our dipole approach.

In Fig. 6 we show the results for the four systems depicted in Fig. 2. For the magnetization in the sample (bottom of Fig. 6) we again find a very good quantitative agreement between the analytic dipole relation Eq. (22) and the full field results. Consequently, the effective magnetization of all particles in the sample is indeed roughly independent of the actual particle distribution Φ_p and can be described very accurately by the dipole approximation. Nevertheless, the respective local magnetization field within each individual particle may fluctuate significantly as can be observed in Fig. 2.

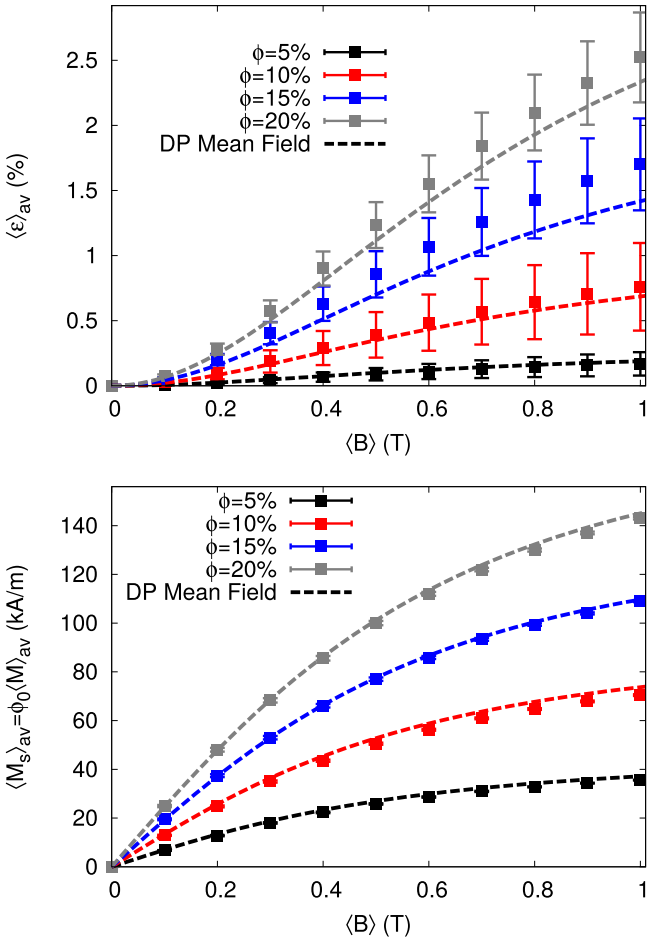

FIG. 5. Same as in Fig. 4 for a saturating magnetization behavior of the embedded particles according to Eq. (4), with $M_\infty = 868\ \mathrm{kA\,m^{-1}}$, $\mu_\mathrm{r} = 27.61$, and $E_\mathrm{m} = 200\ \mathrm{kPa}$.

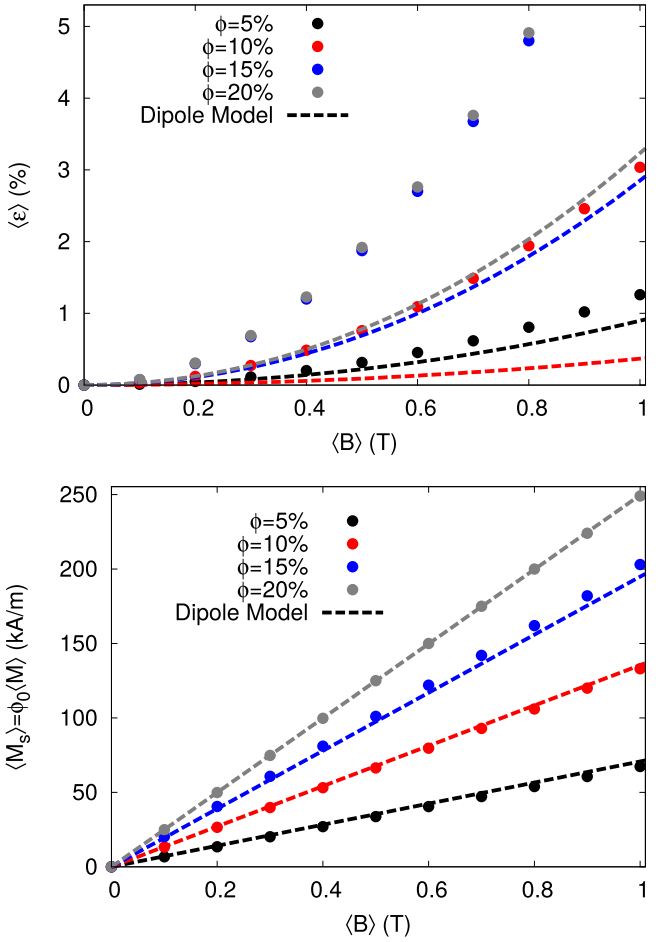

FIG. 6. Comparison of the results for some discrete particle positions according to the four distributions shown in Fig. 2. (top) The effective deformation $\langle\varepsilon\rangle$ in direction of the applied field H_0 ($\langle B\rangle$). (bottom) The corresponding effective magnetization $\langle M_\mathrm{s}\rangle$ in field direction for each sample. We assume linear magnetization with $\mu_\mathrm{r} = 27.61$ and $E_0 = 200\ \mathrm{kPa}$.

In the top of Fig. 6 we plot the predicted effective deformation ε for both approaches. At least qualitatively we always predict elongation in direction of the external field, but the quantitative agreement is very poor. Merely for the first system with $\phi = 5\%$ we find approximately the same quantitative magnetostrictive effect. Another accordance can be identified for the $\phi = 15\%$ and $\phi = 20\%$ systems, where both approaches predict that these systems deform almost identically (with the $\phi = 20\%$ system slightly stronger deformed). But this qualitative accordance seems a pure coincidence, especially if we compare the results for $\phi = 5\%$ and $\phi = 10\%$, where the dipole approach predicts a smaller deformation for $\phi = 10\%$ in clear contradiction to the full field result. Hence, the very good consistency of both approaches predicting the same effective magnetization does not provide an indication for the accuracy of the respective magnetostriction in the case of discrete particle distributions. We will discuss this result in the following.

VI. DISCUSSION

In the present work, we compare a full field and a dipolar mean field approach regarding their predictions for the magnetostrictive response of MSEs with cylindrical inclusions. After a short revision of the basic ideas of the individual modeling strategies, the mean field approach is modified in order to comply with the systems under consideration. The subsequent comparison of the simulation results shows a very good agreement for the average magnetization as well as the average magnetostrictive strains. The predictions of both models nearly coincide for dilute systems with a low particle volume fraction ϕ. Since the influence of an inhomogeneous magnetization increases with ϕ, the accuracy of the mean field approach decreases in microstructures which comprise a higher amount of particles. However, in our work a good accordance up to $\phi = 20\%$ is evident.

A comparison of our full field results with those of the dipole model with discrete particle distributions reveals significant deviations. Although the predictions for the effective magnetization are in good agreement, both approaches entail fundamental differences with regard to the magnetostrictive response. Here, the advantages of the full field approach become apparent: the dipolar-interaction models are not appropriate to predict the behavior of a single MSE with a specific particle distribution. Due to the various simplifying

assumptions in the dipole model (i.e., effective medium, pure affine deformations, homogeneous magnetization fields) it is not surprising that the results in Fig. 6 differ strongly in predicting the magnetostrictive effect. Additionally, the size of a single representative volume element might not be sufficient; see Fig. 2. In contrast, the dipolar mean field model predicts even quantitatively the same magnetostriction as the full field approach statistically averaged over many randomly generated samples. In fact, our work shows that a mean field approach is a modeling strategy which allows us to capture the average behavior of MSEs with a microstructure that can be described by a continuously varying distribution function.

Reference [41] states that dipoles which are distributed discretely on a regular cubic lattice are not a good choice to model amorphous, isotropic materials. The present work additionally suggests that even random irregular discrete distributions of dipoles are not appropriate to describe the composite material behavior. We want to emphasize that there is a fundamental difference between discrete dipole models and dipolar mean field approaches: By "smearing" the dipole field (continuous distribution function) the surrounding dipoles may be anywhere and "each possible position" contributes to the interaction. This way every dipole interacts not only with some other point-like object (with very much "empty" space between the discrete dipoles) but also with rather extended objects (as we effectively also account for contributions away from the center position). This interpretation is additionally supported by our findings that, in the discrete dipole model, a very small displacement of only one or two particles in the sample is sufficient to change the results for the magnetostriction dramatically (up to entire orders of magnitude). Such a particular sensitivity with respect to individual particle positions is not supported by the full field results. Considering for example the moderate statistical error bars in Figs. 4 and 5 for 20 different systems in the full field approach, the standard deviation for the discrete dipole results would largely exceed the actual plot size.

To achieve a better comparability of the mean field and full field approaches in the future, different points have to be worked on. On the one hand, there is no reliable information in how far the widely used assumption of an affine deformation [7–11,13] influences the results derived from the mean field model. Consequently, an implementation permitting a nonaffine deformation within the sample is pursued. On the other hand, the finite element results show that a dipole approximation is not realistic if the magnetizable particles get close to each other. Since this is especially the case in MSEs with a high particle volume fraction, which are frequently examined in experimental studies [47–51], the multipole expansion suggested by Ref. [15] has to be adapted for mutually interacting particles. Until now the computationally intensive full field approach has been applied in a two-dimensional simulation to model infinitely long cylindrical particle inclusions. Such two-dimensional simulations revealed good qualitative agreement with experimental results [27]. MSEs of technical relevance are three dimensional and comprise magnetizable particles with a nearly ellipsoidal or even spherical shape. Since the physical mechanisms in two- and three-dimensional samples are very similar, we believe that the results of both approaches will be comparable also for spherical particle inclusions. Nevertheless, to confirm this assumption the present study has to be repeated for the three-dimensional case.

ACKNOWLEDGMENTS

The present study is funded by the German Research Foundation (DFG), Priority Programme (SPP) 1713, Grants No. GR 3725/7-1 and No. KA 3309/5-1. This support is gratefully acknowledged.

APPENDIX A: ALTERNATIVE DERIVATION FOR TWO-DIMENSIONAL DIPOLES

In the following two alternative ways are presented to obtain the demagnetization field of a dipole in a quasi-2D system.

1. Infinite chain of dipoles

We denote the magnetic field generated by a single point-like magnetic dipole $\boldsymbol{m}$ located at $\boldsymbol{r}_0 = \boldsymbol{0}$ as the dipolar demagnetization field. At any point $\boldsymbol{r} \neq \boldsymbol{r}_0$ it is given by

$$\boldsymbol{H}_\mathrm{d} = -\nabla \psi_\mathrm{m}(\boldsymbol{r}), \tag{A1}$$

where the scalar potential $\psi_\mathrm{m}(\boldsymbol{r})$ fulfills the Laplace equation ($\nabla^2 \psi_\mathrm{m} = 0$) and is given by [32,44]

$$\psi_\mathrm{m}(\boldsymbol{r}) = \frac{\boldsymbol{m} \cdot \boldsymbol{r}}{4\pi r^3}. \tag{A2}$$

Let us consider a long chain of n_z identical magnetic dipoles $\boldsymbol{m}$ arranged in row of length L_z along the z axis with $x_0 = y_0 = 0$. In accordance with our prior assumptions $\boldsymbol{m}$ is oriented perpendicular to the z direction. The line density n_z/L_z determines the "amount of magnetic dipole" in each xy plane at given z. We denote the density of magnetic dipoles per xy plane as $\widetilde{\boldsymbol{m}} = \boldsymbol{m} n_z/L_z$ and a spatial vector in such a plane as $\boldsymbol{s}$. To determine the scalar potential that such a chain of identical dipoles generates at some point $\boldsymbol{r}$ we have to sum up the potential of each dipole in the entire chain. This can be explicitly calculated for arbitrary z and $\boldsymbol{s} \neq \boldsymbol{s}_0$, but we focus on the xy plane midway along the chain. Thus,

$$\psi_\mathrm{m}(\boldsymbol{s}) = \frac{n_z \boldsymbol{m} \cdot \boldsymbol{s}}{4\pi L_z} \int_{-L_z/2}^{Lz/2} \frac{dz}{r^3} = \frac{\widetilde{\boldsymbol{m}} \cdot \boldsymbol{s}}{2\pi} \frac{L_z}{s^2 \sqrt{4s^2 + L_z^2}}. \tag{A3}$$

Note, $r^2 = s^2 + z^2$. For an infinitely long chain (where then any point along the chain is midway) of constant dipole line density $\widetilde{\boldsymbol{m}}$ the last fraction in Eq. (A3) reduces to $1/s^2$. The two-dimensional gradient with respect to $\boldsymbol{s}$ (denoted ∇_2D) determines the demagnetization field generated by such an infinitely long chain of identical dipoles with constant line density:

$$\boldsymbol{H}_\mathrm{d} = -\nabla_\mathrm{2D} \psi_\mathrm{m}(\boldsymbol{s}) = \frac{2(\widetilde{\boldsymbol{m}} \cdot \boldsymbol{s})\boldsymbol{s} - s^2 \widetilde{\boldsymbol{m}}}{2\pi s^4}. \tag{A4}$$

This form is identical to the last term in Eq. (18). Note the necessary change in the units $[1/L_z]$ upon transferring 3D dipoles ($\boldsymbol{m}$) to 2D dipoles ($\widetilde{\boldsymbol{m}} = \boldsymbol{m} n_z/L_z$). Thus, they are fun-

damentally different objects. In our dipolar mean field model [from Eqs. (12) to (18)] this difference is hidden in the dimensionless definition of Φ_p, where local dipoles are interpreted as "smeared" average magnetization fields over the extent of each particle. Magnetization fields are not interpreted differently and do not change their units in varying space dimensions.

2. Homogeneously magnetized circle in two dimensions

To obtain the 2D analog of interacting magnetic dipoles (which is originally only well defined in 3D) in Eq. (18) or Eq. (A4) we "integrated out" the third dimension (z direction). Hence, the dipoles defined in the two-dimensional xy plane, i.e., $z = 0$, implicitly account for the interactions with dipoles (or magnetized matter) out of that plane ($z \neq 0$) as the resultant demagnetization field sums up the effects from all the (identical) xy planes at arbitrary z. In the following we completely disregard the third direction and describe the situation of a homogeneously magnetized circle (radius $r_\mathrm{p} = d_\mathrm{p}/2$) in the xy plane. Similar to the well-known calculations for a homogeneously magnetized sphere in 3D [32] the magnetic scalar potential ψ for a circle fulfills the 2D Laplace equation $\nabla^2_{2\mathrm{D}}\psi_\mathrm{out} = 0$ outside of the circle ($s > r_\mathrm{p}$) and we expand ψ_out in homogeneous harmonic polynomials:

$$0 = \nabla^2_{2\mathrm{D}}\psi_\mathrm{out} = \left(\frac{\partial^2}{\partial s^2} + \frac{\partial}{s\partial s} + \frac{\partial^2}{s^2\partial\theta^2}\right)\sum_{n=0}^{\infty} c_n \frac{q_n(\theta)}{s^n}. \quad \text{(A5)}$$

Here, the two-dimensional Laplace operator is given in polar coordinates. The coefficients c_n will be determined later via boundary conditions. The angular functions $q_n(\theta)$ are found straightforward after taking the partial derivatives with respect to s in Eq. (A5). To fulfill the Laplace equation they must be of the form $q_n(\theta) = \cos(n\theta)$. Note that, with a three-dimensional Laplacian in Eq. (A5) (e.g., for a sphere), the q_n are formed by the ordinary spherical harmonics which can be reduced to the Legendre polynomials $P_l(\cos\theta)$ since the solution must be independent of the azimuthal angle. Then $q_n(\theta) = P_{n-1}(\cos\theta)$. Inside the circle the magnetic field $\boldsymbol{H} = \boldsymbol{H}_0 + \boldsymbol{H}_\mathrm{d}$ is considered homogeneous over the entire extent of the circle. Thus the medium is homogeneously magnetized in direction of $\boldsymbol{H}$ ($\boldsymbol{M} \parallel \boldsymbol{H} = \text{const.}$). Therefore,

$$\psi_\mathrm{in}(\boldsymbol{s}) = C\boldsymbol{M}\cdot\boldsymbol{s} = CMs\cos\theta, \quad \text{(A6)}$$

where θ denotes the angle between $\boldsymbol{M}$ and $\boldsymbol{s}$. The coefficient C is determined by the continuity condition $\Psi_\mathrm{in}(s = r_\mathrm{p}) = \Psi_\mathrm{out}(s = r_\mathrm{p})$ revealing only the $q_{n=1}$ term that survives in Ψ_out with $c_1 = CMr_\mathrm{p}^2$. The magnetic field at the circle boundary displays a jump equal to the surface magnetic charge density $\sigma = \boldsymbol{n}\cdot\boldsymbol{M}$, with $\boldsymbol{n}$ being the unit normal vector at the circle boundary. This implies the following condition:

$$\sigma = M\cos\theta = \left(\frac{\partial\Psi_\mathrm{in}}{\partial s} - \frac{\partial\Psi_\mathrm{out}}{\partial s}\right)_{s=r_\mathrm{p}} = 2CM\cos\theta. \quad \text{(A7)}$$

Hence, we find $C = 1/2$ and the demagnetization factor of a circle is identical to that of an infinitely long cylinder being homogeneously magnetized perpendicular to its main axis ($N_\mathrm{d} = 1/2$). The scalar potential outside of the circle reads finally

$$\Psi_\mathrm{out}(\boldsymbol{s}) = \frac{r_\mathrm{p}^2 M\cos\theta}{2s} = a_\mathrm{p}\frac{\boldsymbol{M}\cdot\boldsymbol{s}}{2\pi s^2}. \quad \text{(A8)}$$

Here, $a_\mathrm{p} = \pi r_\mathrm{p}^2$ denotes the circle area, or analogously the cylindrical cross section, and the 2D dipole is the sum of the (homogeneous) magnetization field in the circle $\tilde{\boldsymbol{m}} = \int_{a_\mathrm{p}} d^2s\boldsymbol{M} = a_\mathrm{p}\boldsymbol{M}$ [compare with Eq. (10)]. Hence, Eq. (A8) is identical to Eq. (A3) in the limit of an infinitely long chain $L_z \to \infty$.

APPENDIX B: DISCRETE DISTRIBUTION OF PARTICLES

For a discrete allocation of the magnetizable particles (monodisperse, with the area $a_i = a_\mathrm{p}$ for all particles) we insert a discrete dimensionless distribution of the form $\Phi_\mathrm{p} = \sum_{i=1}^{\mathcal{N}_\mathrm{p}} a_\mathrm{p}\delta(\boldsymbol{s} - \boldsymbol{s}_i)$ into our dipolar mean field approach (18) and obtain a summation:

$$\boldsymbol{H}_{\mathrm{d}_j} = -N_\mathrm{d}\boldsymbol{M}_j + \frac{a_\mathrm{p}}{2\pi}\sum_{i=1}^{\mathcal{N}_\mathrm{p}}\frac{2(\boldsymbol{M}_i\cdot\boldsymbol{s}_{ij})\boldsymbol{s}_{ij} - s_{ij}^2\boldsymbol{M}_j}{s_{ij}^4}. \quad \text{(B1)}$$

Here, $\boldsymbol{H}_{\mathrm{d}_j}$ denotes the (locally constant) demagnetization field over the extent of particle j, $\boldsymbol{M}_j$ is the (constant) magnetization in particle j, and $\boldsymbol{s}_{ij} = \boldsymbol{s}_i - \boldsymbol{s}_j$. We consider now only linear magnetization behavior ($\boldsymbol{M}_j = \chi\boldsymbol{H}_j$). With $\boldsymbol{H}_j = \boldsymbol{H}_0 + \boldsymbol{H}_{\mathrm{d}_j}$, Eq. (B1) forms a coupled set of $2\mathcal{N}_\mathrm{p}$ equations. For a given distribution (i.e., Fig. 2, periodically continued in x and y) we solve this set self-consistently. The effective magnetization $\langle\boldsymbol{M}_\mathrm{s}\rangle$ of all particles per sample volume V_s, respectively per sample area $A_\mathrm{s} = L_\parallel L_\perp$, is then

$$\langle\boldsymbol{M}_\mathrm{s}\rangle = \frac{1}{V_\mathrm{s}}\int_{V_\mathrm{s}} d^3r\boldsymbol{M} = \frac{a_\mathrm{p}}{A_\mathrm{s}}\sum_{i=1}^{\mathcal{N}_\mathrm{p}}\boldsymbol{M}_i = \phi\sum_{i=1}^{\mathcal{N}_\mathrm{p}}\frac{\boldsymbol{M}_i}{\mathcal{N}_\mathrm{p}} = \phi\langle\boldsymbol{M}\rangle. \quad \text{(B2)}$$

The magnetic energy is obtained from Eq. (30). For an affine deformation ε we reallocate each particle accordingly and compare the result to the undeformed sample. Minimizing Eq. (17) we find the equilibrium, or effective, deformation $\langle\varepsilon\rangle$ of the MSE sample.

[1] O. V. Stolbov, Yu. L. Raikher, and M. Balasoiu, Modelling of magnetodipolar striction in soft magnetic elastomers, Soft Matter **7**, 8484 (2011).

[2] G. Schubert, Ph.D. thesis, University of Glasgow, 2014, http://theses.gla.ac.uk/5475/3/2014schubertphd_Redacted.pdf.

[3] T. F. Tian, W. H. Li, and Y. M. Deng, Sensing capabilities of graphite-based MR elastomers, Smart Mater. Struct. **20**, 025022 (2011).

[4] H. Böse, R. Rabindranath, and J. Ehrlich, Soft magnetorheological elastomers as new actuators for valves, J. Intell. Mater. Syst. Struct. **23**, 989 (2012).

[5] J. D. Carlson and M. R. Jolly, MR fluid, foam and elastomer devices, Mechatronics **10**, 555 (2000).

[6] S. Sassi, K. Cherif, L. Mezghani, M. Thomas, and A. Kotrane, An innovative magnetorheological damper for automotive suspension: From design to

experimental characterization, Smart Mater. Struct. **14**, 811 (2005).

[7] M. R. Jolly, J. D. Carlson, B. C. Munoz, and T. A. Bullions, The magnetoviscoelastic response of elastomer composites consisting of ferrous particles embedded in a polymer matrix, J. Intell. Mater. Syst. Struct. **7**, 613 (1996).

[8] Y. Han, W. Hong, and L. E. Faidley, Field-stiffening effect of magneto-rheological elastomers, Int. J. Solids Struct. **50**, 2281 (2013).

[9] Y. Han, A. Mohla, X. Huang, W. Hong, and L. E. Faidley, Magnetostriction and field stiffening of magneto-active elastomers, Int. J. Appl. Mech. **07**, 1550001 (2015).

[10] D. Ivaneyko, V. P. Toshchevikov, M. Saphiannikova, and G. Heinrich, Magneto-sensitive elastomers in a homogeneous magnetic field: A regular rectangular lattice model, Macromol. Theory Simul. **20**, 411 (2011).

[11] D. Ivaneyko, V. Toshchevikov, M. Saphiannikova, and G. Heinrich, Mechanical properties of magneto-sensitive elastomers: Unification of the continuum-mechanics and microscopic theoretical approaches, Soft Matter **10**, 2213 (2014).

[12] G. Pessot, P. Cremer, D. Y. Borin, S. Odenbach, H. Löwen, and A. M. Menzel, Structural control of elastic moduli in ferrogels and the importance of non-affine deformations, J. Chem. Phys. **141**, 124904 (2014).

[13] D. Romeis, V. Toshchevikov, and M. Saphiannikova, Elongated micro-structures in magneto-sensitive elastomers: A dipolar mean field model, Soft Matter **12**, 9364 (2016).

[14] E. E. Keaveny and M. R. Maxey, Modeling the magnetic interactions between paramagnetic beads in magnetorheological fluids, J. Comput. Phys. **227**, 9554 (2008).

[15] A. M. Biller, O. V. Stolbov, and Yu. L. Raikher, Modeling of particle interactions in magnetorheological elastomers, J. Appl. Phys. **116**, 114904 (2014).

[16] A. M. Biller, O. V. Stolbov, and Yu. L. Raikher, Mesoscopic magnetomechanical hysteresis in a magnetorheological elastomer, Phys. Rev. E **92**, 023202 (2015).

[17] A. M. Biller, O. V. Stolbov, and Yu. L. Raikher, Dipolar models of ferromagnet particles interaction in magnetorheological composites, J. Optoelectron. Adv. Mater. **17**, 1106 (2015).

[18] R. Bustamante, Transversely isotropic nonlinear magneto-active elastomers, Acta Mech. **210**, 183 (2010).

[19] K. Danas, S. V. Kankanala, and N. Triantafyllidis, Experiments and modeling of iron-particle-filled magnetorheological elastomers, J. Mech. Phys. Solids **60**, 120 (2012).

[20] A. Dorfmann and R. W. Ogden, Magnetoelastic modeling of elastomers, Eur. J. Mech., A **22**, 497 (2003).

[21] K. Haldar, B. Kiefer, and A. Menzel, Finite element simulation of rate-dependent magneto-active polymer response, Smart Mater. Struct. **25**, 104003 (2016).

[22] S. V. Kankanala and N. Triantafyllidis, On finitely strained magnetorheological elastomers, J. Mech. Phys. Solids **52**, 2869 (2004).

[23] Yu. L. Raikher and O. V. Stolbov, Numerical modeling of large field-induced strains in ferroelastic bodies: A continuum approach, J. Phys.: Condens. Matter **20**, 204126 (2008).

[24] A. Javili, G. Chatzigeorgiou, and P. Steinmann, Computational homogenization in magneto-mechanics, Int. J. Solids Struct. **50**, 4197 (2013).

[25] K. A. Kalina, P. Metsch, and M. Kästner, Microscale modeling and simulation of magnetorheological elastomers at finite strains: A study on the influence of mechanical preloads, Int. J. Solids Struct. **102-103**, 286 (2016).

[26] M.-A. Keip and M. Rambausek, A multiscale approach to the computational characterization of magnetorheological elastomers, Int. J. Numer. Methods Eng. **107**, 338 (2016).

[27] P. Metsch, K. A. Kalina, C. Spieler, and M. Kästner, A numerical study on magnetostrictive phenomena in magnetorheological elastomers, Comput. Mater. Sci. **124**, 364 (2016).

[28] P. Ponte Castañeda and E. Galipeau, Homogenization-based constitutive models for magnetorheological elastomers at finite strain, J. Mech. Phys. Solids **59**, 194 (2011).

[29] J. Schröder, M. Labusch, and M.-A. Keip, Algorithmic two-scale transition for magneto-electro-mechanically coupled problems: FE^2-scheme: Localization and homogenization, Comput. Methods Appl. Mech. Eng. **302**, 253 (2016).

[30] F. Vogel, R. Bustamante, and P. Steinmann, On some mixed variational principles in magneto-elastostatics, Int. J. Non-Linear Mech. **51**, 157 (2013).

[31] C. Spieler, M. Kästner, J. Goldmann, J. Brummund, and V. Ulbricht, XFEM modeling and homogenization of magnetoactive composites, Acta Mech. **224**, 2453 (2013).

[32] J. D. Jackson, *Classical Electrodynamics*, 3rd ed. (Wiley, New York, 1999).

[33] C. Spieler, P. Metsch, M. Kästner, and V. Ulbricht, Microscale modeling of magnetoactive composites undergoing large deformations, Technische Mechanik **34**, 39 (2014).

[34] S. R. de Groot and L. G. Suttorp, *Foundations of Electrodynamics* (North-Holland, Amsterdam, 1972).

[35] A. C. Eringen and G. A. Maugin, *Electrodynamics of Continua I: Foundations and Solid Media* (Springer, New York, 1990).

[36] R. Hill, Elastic properties of reinforced solids: Some theoretical principles, J. Mech. Phys. Solids **11**, 357 (1963).

[37] E. Galipeau and P. P. Castañeda, A finite-strain constitutive model for magnetorheological elastomers: Magnetic torques and fiber rotations, J. Mech. Phys. Solids **61**, 1065 (2013).

[38] E. Galipeau, Ph.D. thesis, University of Pennsylvania, 2012, http://repository.upenn.edu/edissertations/634/.

[39] E. Galipeau, S. Rudykh, G. deBotton, and P. Ponte Castañeda, Magnetoactive elastomers with periodic and random microstructures, Int. J. Solids Struct. **51**, 3012 (2014).

[40] R. A. Anderson, Mechanical stress in a dielectric solid from a uniform electric field, Phys. Rev. B **33**, 1302 (1986).

[41] Y. M. Shkel and D. J. Klingenberg, Electrostriction of polarizable materials: Comparison of models with experimental data, J. Appl. Phys. **83**, 7834 (1998).

[42] L. Treloar, *The Physics of Rubber Elasticity*, Monographs on the physics and chemistry of materials (Oxford University Press, Oxford, 2005).

[43] H. M. Smallwood, Limiting law of the reinforcement of rubber, J. Appl. Phys. **15**, 758 (1944).

[44] L. Landau and E. Lifschitz, *Electrodynamics of Continuous Media* (Pergamon Press, Oxford, 1960).

[45] S. Torquato, *Random Heterogeneous Materials*, 1st ed. (Springer, New York, 2002).

[46] J. A. Osborn, Demagnetizing factors of the general ellipsoid, Phys. Rev. **67**, 351 (1945).

[47] S. Abramchuk, E. Kramarenko, G. Stepanov, L. V. Nikitin, G. Filipcsei, A. R. Khokhlov, and M. Zrínyi, Novel highly elastic

magnetic materials for dampers and seals: Part i. preparation and characterization of the elastic materials, Polym. Adv. Technol. **18**, 883 (2007).

[48] S. Abramchuk, E. Kramarenko, D. Grishin, G. Stepanov, L. V. Nikitin, G. Filipcsei, A. R. Khokhlov, and M. Zrínyi, Novel highly elastic magnetic materials for dampers and seals: Part ii. material behavior in a magnetic field, Polym. Adv. Technol. **18**, 513 (2007).

[49] J. M. Ginder, M. E. Nichols, L. D. Elie, and J. L. Tardiff, Magnetorheological elastomers: Properties and applications, in *Smart Structures and Materials 1999: Smart Materials Technologies*, Vol. 3675, edited by M. R. Wuttig (Proc. SPIE, Newport Beach, California, 1999), pp. 131–138.

[50] G. V. Stepanov, D. Y. Borin, Yu. L. Raikher, P. V. Melenev, and N. S. Perov, Motion of ferroparticles inside the polymeric matrix in magnetoactive elastomers, J. Phys.: Condens. Matter **20**, 204121 (2008).

[51] G. Y. Zhou and Z. Y. Jiang, Deformation in magnetorheological elastomer and elastomer–ferromagnet composite driven by a magnetic field, Smart Mater. Struct. **13**, 309 (2004).